ABSTRACT

Title of dissertation: NONLINEAR PULSE PROPAGATION THROUGH AN OPTICAL FIBER: THEORY AND EXPERIMENT

Bhaskar Khubchandani
Doctor of Philosophy, 2004

Dissertation directed by: Professor Rajarshi Roy
Department of Physics

Pulse propagation through optical fibers is studied for two different phenomena: (i) the evolution of four-wave-mixing and (ii) the interplay between self- and cross-phase modulation for ultra-short pulses in a polarization maintaining fiber.

For the four-wave-mixing case, we present the results of a study of the dynamical evolution of multiple four-wave-mixing processes in a single-mode optical fiber with spatially and temporally δ-correlated phase noise. A nonlinear Schrödinger equation (NLSE) with stochastic phase fluctuations along the length of the fiber is solved using the Split-Step Fourier method. Good agreement is obtained with previous experimental and computational results based on a truncated-ODE model in which stochasticity was seen to play a key role in determining the nature of the dynamics. The full NLSE allows for simulations with high frequency resolution (60 MHz) and frequency span (16 THz) compared to the truncated ODE model (300 GHz and 2.8 THz, respectively), thus enabling a more detailed comparison with observations. Fluctuations in the refractive index of the fiber core are found to be

a possible source for this phase noise. It is found that index fluctuations as small as 1 part per billion are sufficient to explain observed features of the evolution of the four-wave-mixing sidebands. These measurements and numerical models thus may provide a technique for estimating these refractive index fluctuations which are otherwise difficult to measure.

For the case of self- and cross-phase modulation, the evolution of orthogonal polarizations of asymmetric femtosecond pulses (810 nm) propagating through a birefringent single-mode optical fiber (6.9 cm) is studied both experimentally (using GRENOUILLE) and numerically (using a set of coupled NLSEs). A linear optical spectrogram representation is derived from the electric field of the pulses and juxtaposed with the optical spectrum and optical time-trace. The simulations are in good qualitative agreement with the experiments. Input temporal pulse asymmetry is found to be the dominant cause of output spectral asymmetry. The results indicate that it is possible to modulate short pulses both temporally and spectrally by passage through polarization maintaining optical fibers with specified orientation and length.

NONLINEAR PULSE PROPAGATION THROUGH AN OPTICAL FIBER : THEORY AND EXPERIMENT

by

Bhaskar Khubchandani

Dissertation submitted to the Faculty of the Graduate School of the
University of Maryland, College Park in partial fulfillment
of the requirements for the degree of
Doctor of Philosophy
2004

Advisory Committee:
Professor Rajarshi Roy, Chair/Advisor
Dr. Parvez N. Guzdar, Co-Advisor
Professor Robert W. Gammon
Professor Thomas Antonsen
Professor Edward Ott

Preface

If needed.

Foreword

If needed.

Dedication

If needed.

Acknowledgments

I owe my gratitude to all the people who have made this thesis possible and because of whom my graduate experience has been one that I will cherish forever.

First and foremost I'd like to thank my advisor, Professor Rajarshi Roy for giving me an invaluable opportunity to work on challenging and extremely interesting projects over the past four years. He has always made himself available for help and advice and there has never been an occasion when I've knocked on his door and he hasn't given me time. It has been a pleasure to work with and learn from such an extraordinary individual.

I would also like to thank my co-advisor, Dr. Parvez Guzdar. Without his extraordinary theoretical ideas and computational expertise, this thesis would have been a distant dream. Thanks are due to Professor Robert Gammon, Professor Edward Ott and Professor Thomas Antonsen for agreeing to serve on my thesis committee and for sparing their invaluable time reviewing the manuscript.

My colleagues at the nonlinear optics laboratory have enriched my graduate life in many ways and deserve a special mention. David DeShazer helped me start-off by rewriting the basic simulation code in a user-friendly format. Christian Silva provided help by setting up the GRENOUILLE apparatus and performing some of the simulations. My interaction with Rohit Tripathi, Ryan McAllister, Vasily Dronov, Min-Young Kim, Elizabeth Rogers, William Ray, Jordi Garcia Ojalvo, Riccardo Meucci, Atsushi Uchida, and Fabian Rogister has been very fruitful. I'd also like to thank Wing-Shun Lam and Benjamin Zeff for providing the LaTex style files

for writing this thesis.

I would also like to acknowledge help and support from some of the staff members. Donald Martin's technical help is highly appreciated, as is the computer hardware support from Edward Condon, LaTex and software help from Dorothea Brosius and purchasing help from Nancy Boone.

I owe my deepest thanks to my family - my mother and father who have always stood by me and guided me through my career, and have pulled me through against impossible odds at times. Words cannot express the gratitude I owe them. I would also like to thank Dr. Mohan Advani, Dr. Vasudeo Paralikar and Dr. Vinod Chaugule who are like family members to me.

My housemates at my place of residence have been a crucial factor in my finishing smoothly. I'd like to express my gratitude to Sivasankar Pandeti, Jayakumar Patil, Amit Trehan and Punyaslok Purakayastha for their friendship and support.

I would like to acknowledge financial support from the Office of Naval Research (ONR), Physics, for all the projects discussed herein.

It is impossible to remember all, and I apologize to those I've inadvertently left out.

Lastly, thank you all and thank God!

Table of Contents

List of Tables

List of Figures

List of Abbreviations

AAA	Antiaircraft artillery
ABCCC	Airborne Battlefield Command and Control Center
AEHF	Advanced Extremely High Frequency
AGM	Air-to-ground guided missile
AIT	Assembly, Integration, and Testing
AOR	Area of Responsibility
APAM	Anti-personnel, anti-material
ASOC	Air Support Operations Center
ATACM	Army Tactical Missile System
ATO	Air Tasking Order
AWACS	Airborne Warning and Control System
BAT	Brilliant Ani-Armor Submunition
BDA	Bomb-damage assessment
BFT	Blue Force Tracking
BLOS	Beyond Line-of-Sight
BMD	Ballistic Missile Defense
C^3	Command, Control, and Communications
CAFMS	Computer-aided Force Management System
CALCM	Conventional Air-Launched Cruise Missile
CBU	Cluster Bomb Unit
CCAFS	Cape Canaveral Air Force Station
CENTAF	CENTCOM's Air Force component
CENTCOM	U.S. Central Command
CINC	Commander-in-Chief
CONUS	Continental United States
DAGR	Defense Advanced GPS Reciever
DMA	Defense Mapping Agency
DOD	Department of Defense
DOP	Dilution of Precision
DOT	Department of Transportation
DSMAC	Digital Scene Mapping Area Correlator
EFOG-M	Enhanced Fiber Optic Guided Missile
FAA	Federal Aviation Administration
FLIR	Forward-looking infrared

GAM	Global Positioning System Aided Munition
GPS	Global Positioning System
GWAPS	Gulf War Air Power Survey
HARM	High-Speed Antiradiation Missile
HEO	Highly Elliptical Orbit
IADS	Integrated Air Defense System
ICBM	Inter-Continental Ballistic Missile
INS	Inertial navigation system
IIR	Imaging infrared
IR	Infrared
ISR	Intelligence, Surveillance, and Reconnaissance
JDAM	Joint Direct Attack Munition
JFC	Joint Force Commander
JSOW	Joint Standoff Weapon
LANTIRN	Low-Altitude Navigation and Targeting Infrared for Night System
LEO	Low Earth Orbit
LGB	Laser-guided bomb
MAJIC	Microsatellte Area-Wide Joint Information Communication
MARCENT	CENTCOM's Marine component
MARS	Mid-Atlantic Regional Spaceport
MLRS	Multiple Launch Rocket System
MUOS	Mobile User Objective System
NASA	National Aeronautics and Space Administration
NAVCENT	CENTCOM's Navy component
NPOESS	National Polar-Orbiting Operational Environmental Satellite System
ORS	Opertionally Responsive Space
ORSO	Operationally Responsive Space Office
PDOP	Position Dilution of Precision
PGM	Precision-guided munition
P^3I	Preplanned Product Improvement
PnP	Plug and Play

PnPSat	Plug and Play Satellite
PPS	Precise Positioning Service
RCS	Radar cross section
SA	Situational Awareness
SADARM	Sense and Destroy Armor Munition
SAM	Surface-to-air missile
SAR	Synthetic aperture radar
SBIRS	Space Based Infrared System
SEAD	Suppression of enemy air defenses
SFW	Sensor Fuzed Weapon
SIGINT	Signal Intelligence
SLAM	Standoff Land Attack Missile
SLAM-ER	SLAM-Expanded Response
SpaceX	Space Exploration Technologies Corporation
SPS	Standard Positioning Service
TACC	Tactical Air Control Center
TACS	Tactical Air Control System
TACP	Tactical Air Control Party
TASM	Tomahawk Anti-Ship Missile
TBIP	Tomahawk Baseline Improvement Program
TERCOM	Terrain Contour Mapping
TFR	Terrain-following radar
TLAM	Tomahawk Land Attack Missile
USAF	U.S. Air Force
VAFB	Vandenberg Air Force Base
WGS	Wideband Global SATCOM

Chapter 3: Direct measurement of a Feshbach resonance in ^{40}K via observation of *s-wave scattering*

3.1 Introduction

Feshbach resonances are widely used for tuning the interaction strength in ultracold atomic gases. They have been particularly instrumental in the study of interactions and interaction-dependent processes in cold Fermi gases. In contrast to atomic Bose-Einstein condensates (BECs), where even weak interactions play a crucial role, for example giving rise to their characteristic Thomas-Fermi density profiles [**?**], interractions must compete with the Fermi energy before becoming relevant. Practically speaking, the density of Fermi clouds is typically ∼1000 times less than that of BECs [1], making it necessary to enhance the strength of interactions in order to observe significant interaction effects [**?**]. The tunability of interactions provided by Feshbach resonances has allowed for creation of molecular Bose-Einstein condensates from Fermi gases [**?**, **?**, **?**] as well as observation of the phase transition from the Bardeen-Cooper-Schrieffer (BCS) superconduting regime to the BEC regime at sufficiently low temperatures [**?**, **?**, **?**, **?**].

[1] This is not the case for recently realized erbium and dysprosium DFGs [**?**, **?**], where strong dipolar interactions are present.

A Feshbach resonance occurs when a diatomic molecular state energetically approaches the two-atom continuum [?, ?]. In experiment, the relative energy of the free atomic states in two hyperfine sublevels and the molecular state is defined by a bias magnetic field. Consequently, the Feshbach resonance can be accessed by changing the bias field. In the simple case where there are no inelastic two-body channels, such as for the ^{40}K resonance discussed in this work, the effect of the resonance on the scattering length between two free atoms is [?]

$$a(B) = a_{\mathrm{bg}} \left(1 - \frac{\Delta}{B - B_0}\right), \tag{3.1}$$

where a_{bg} is the background scattering length, Δ is the width of the resonance, and B_0 is the field value at which the resonance occurs. The scattering length diverges at the resonance.

The exact value of the resonant field B_0 is difficult to calculate analytically and is commonly computed via numerical models based on experimental input parameters [?, ?, ?] or determined experimentally [?, ?]. Many experimental techniques have been used to characterize Feshbach resonances, including the observation of atom loss due to three-body inelastic scattering, measurement of re-thermalization timescales, and anisotropic expansion of the cloud upon release from a confining potential, all of which infer the elastic scattering cross section from collective behavior of the cloud [?, ?, ?].

Here we used direct scattering as a primary probe of the location and width of a Feshbach resonance. We collided pairs of ultra-cold Fermi gases and directly imaged the resulting s-wave scattered atoms as a function of magnetic field strength.

This allowed us to observe the enhancement in scattering without relying on proxy effects. We measured the fraction of atoms scattered during the collision, and from this fraction deduced the resonant magnetic field and the width of the resonance.

In our dilute DFGs, even with the resonant enhancement of the scattering cross section, only a small fraction of the atoms scattered as the clouds passed through each other. This made direct detection of scattered atoms difficult due to detection uncertainty that disproportionately affected regions of low atomic density. To optimize the signal-to-noise ratio (SNR) for low atom numbers, we absorption imaged with fairly long, high-intensity pulses — a non-standard regime, where the atoms acquired a velocity during imaging and the resulting Doppler-shift was non-negligible. Simulation of the absorption imaging process was necessary for an accurate interpretation of these images. Using the simulation-corrected images, we extracted the fraction of atoms scattered in our collision experiment.

This paper is divided into two parts. In the first, we study absorption imaging in the presence of a significant time-dependent Doppler shift and show how we use our results to interpret data. In the second, we describe our s-wave scattering experiment and extract a measure of the location and width of the Feshbach resonance in ^{40}K.

3.2 Experimental setup

In this section we describe our Fermi scattering experiment. We collided two counter-propagating ^{40}K clouds and observed the resulting s-wave halo of scattered

atoms. We measured the dependence of the scattered atomic fraction on the bias magnetic field in the vicinity of the Feshbach resonance. We used this data to extract the location of the magnetic fields resonance of 20.206(15) mT and a width of 1.0(5) mT, similar to the accepted values of 20.210(7) mT and 0.78(6) mT [**?**].

We prepared clouds of cold ^{40}K atoms in a hybrid ^{40}K and ^{87}Rb apparatus, previously described in [**?**, **?**, **?**]. We used a Zeeman slower to slow both species before capturing in a magneto-optical trap (MOT). After 7 s seconds of MOT loading ^{40}K followed by 1.5 s of loading both ^{40}K and ^{87}Rb, we cooled both species in optical molasses for 2 ms. We optically pumped both species into their maximally stretched magnetically trappable states, $|F = 9/2, m_F = 9/2\rangle$ for ^{40}K and $|F = 2, m_F = 2\rangle$ for ^{87}Rb. Both species were then loaded into a quadrupole magnetic trap with a ≈ 7.68 mT/cm gradient along $\mathbf{e_z}$, and cooled evaporatively via forced RF evaporation, sweeping the RF frequency from 18 MHz to 2 MHz in 10 s. The magnetic trap was plugged by a $\lambda = 532$ nm beam, tightly focused to ≈ 30 μm and ≈ 5 W in power, providing a repulsive potential around the zero field point to prevent Majorana losses. Since the ^{40}K atoms were spin polarized and therefore only interacted by the strongly suppressed p-wave interactions, they re-thermalized only due to sympathetic cooling with ^{87}Rb atoms.

We then loaded the atoms into a crossed optical dipole trap, provided by a 1064 nm fiber laser, and continued evaporative cooling by slowly ramping down the dipole trap to trap frequencies of $(\omega_x, \omega_y, \omega_z)/2\pi = (39, 42, 124)$ Hz in the three spatial directions, while also turning off the quadrupole field. We then used adiabatic rapid passage (ARP) to transfer the ^{87}Rb atoms from the $|F = 2, m_F = 2\rangle$

state to the $|F = 1, m_F = -1\rangle$ absolute ground state via 6.8556 GHz microwave coupling (20.02 MHz from the zero field resonance) followed by a magnetic field sweep from -0.469 mT to -0.486 mT in 50 ms. This state was chosen to minimize spin changing collisions with ^{40}K atoms during any further evaporation [**?**]. We then briefly applied an on-resonant probe laser, ejecting any remaining ^{87}Rb atoms in the $F = 2$ manifold from the trap. We again used ARP to transfer the ^{40}K atoms into the $|F = 9/2, m_F = -9/2\rangle$ state by using a 3.3 MHz rf field and sweeping the bias magnetic field from -0.518 mT to -0.601 mT in 150 ms.

Following the state transfer, we had two versions of the protocol – one for approaching the Feshbach resonance from higher fields and one for approaching it from lower fields. For approaching the resonance from lower fields, we proceeded by ramping the bias magnetic field to 19.05 mT, turning on a 42.42 MHz RF field, and then sinusoidally modulating the bias field at 125 Hz for 0.5 s, with a 0.14 mT amplitude, decohering the ^{40}K state into an equal mixture of $|F = 9/2, m_F = -9/2\rangle$ and $|F = 9/2, m_F = -7/2\rangle$. For approaching the resonance from higher fields, the same was done at a bias field of 21.71 mT and an RF frequency of 112.3 MHz. The depolarization allowed the ^{40}K atoms to interact and re-thermalize, allowing us to further evaporate in the dipole trap [**?**]. Since ^{87}Rb is heavier than ^{40}K, we were able to evaporate the ^{40}K atoms past the point where ^{87}Rb atoms were no longer suspended against gravity and had been completely removed. These hyperfine states of ^{40}K were then used to study their Feshbach resonance.

After evaporation, we ramped the bias field in a two-step fashion to the desired value B near the Feshbach resonance. We approached the field using a large pair

of coils in Helmholtz configuration (0.19 mT/A) to bring the magnetic field to a setpoint 0.59 mT away from B, $B - 0.59$ mT when approaching from below and $B + 0.59$ mT from above. We held the atoms at this field for 100 ms to allow the eddy currents induced by the large coils to settle, and then used a lower inductance (0.017 mT/A) set of Helmholtz coils to quickly change the field the remaining 0.59 mT. This allowed us to study the resonance from both sides without the added losses associated with going through the resonance [**?**].

Once at the intended bias field, we split the cloud into two spatially overlapping components with opposing momenta and observed scattering as they moved through each other and separated. These counterpropagating components were created using an $8E_{\mathrm{L}}$ deep near resonant (λ_{L}=766.704 nm) 1-d retro-reflected optical lattice, where $E_{\mathrm{L}} = \hbar^2 k_{\mathrm{L}}^2 / 2m_{\mathrm{K}}$ is the lattice recoil energy and $\hbar k_{\mathrm{L}} = 2\pi\hbar/\lambda$ is the recoil momentum. We rapidly pulsed this lattice on and off with a double-pulse protocol [**?**,**?**]. The pulse sequence was optimized to transfer most of the atoms into the $\pm 2\hbar k_{\mathrm{L}}$ momentum states. Since the initial Fermi gas had a wide momentum spread (in contrast to a BEC, which has a very narrow momentum spread), and the lattice pulsing is a momentum dependent process [**?**], not all the atoms were transferred into the target momentum states. We optimized our pulse times to minimize the atoms remaining in the zero momentum state. The optimized pulse times were 23 μs for the first pulse, 13 μs off interval, and 12 μs for the second pulse [**?**].

We then released the atoms from the trap and allowed 1 ms for the two opposite momentum states within the cloud to pass through each other, scattering on the way. For the data taken coming from below the Feshbach resonance, we then simply

ramped down the field and imaged the atoms. For the data taken coming from above the Feshbach resonance, we ramped the field back up, retreating through the resonance if it had been crossed and thereby dissociating any molecules that were created, and then quickly ramped the field back down and imaged the atoms. We used a 40 μs imaging pulse with $I_0/I_{\rm sat} \approx 0.6$ at the center of the probe laser.

The total time-of-flight, the time from the moment the atoms were released from the trap to when they were imaged, was $t_{TOF} = 6.8$ ms. In such an image, the observed atomic position is determined by the initial velocity upon release from the trap, along with the time-of-fligt time t_{TOF}. Therefore, this technique measures the momentum and not the position distribution of the atoms.

The magnetic fields produced by our coils in the regime of interest were independently calibrated by rf-spectroscopy. We prepared ^{40}K atoms in the $|F = 9/2, m_F = -9/2\rangle$ state and illuminated them with and rf-field with some frequency ν_{rf}. We then ramped our high-inductance coils to variable set points, followed by an adiabatic 250μs ramp of 2.84 mT in the lower inductance coils. We then used Stern-Gerlach and observed the fractional population in the $|F = 9/2, m_F = -9/2\rangle$ and $|F = 9/2, m_F = -7/2\rangle$ states as a function of the high-inductance coil current. We fit the fractional population curve to a Gaussian, and considered the center of the fit to be on-resonant, with an uncertainty given by the Gaussian width. We used the Breit-Rabi formula to determine the resonant field value at ν_{rf}. We did this for 5 different rf frequencies, and acquired a field calibration with an uncertainty of 0.3 mT, which was included in the listed uncertainty on the center field of the Feshbach resonance.

3.3 Methods

We first processed each image by comparing the obsereved ODs to simulations taking into account the recoil induced detuning as described in Sec. **??**. An example of images before and after processing are shown in Fig. 1. To improve the signal and mitigate our shot to shot number fluctuations, we took 15 nominally identical images for each data point.

We counted the fraction of atoms that experienced a single scattering event for each of the fifteen images at a given bias magnetic field. Single scattering events are easily identified, as two atoms that scatter elastically keep the same amplitude of momentum, but depart along an arbitrary direction. Therefore, an atom traveling at $2\hbar k_{\mathrm{L}}$ to the right that collides elastically with an atom traveling at $-2\hbar k_{\mathrm{L}}$ to the left will depart with equal and opposite momenta $2\hbar k_{\mathrm{L}}$ at an arbitrary angle, and in a time of flight image such atoms will lie in a spherical shell, producing the scattering halo pictured in Fig. 2(a).

Absorption images captured the integrated column density along $\mathbf{e_z}$, a projected 2D atomic distribution. To extract the radial dependence of the 3D distribution from the 2D image, we performed a standard inverse Abel transform. The inverse Abel transform assumes cylindrical symmetry, which was present in our case, with the axis of symmetry along $\mathbf{e_x}$, defined by the lattice. We neglect the initial asymmetry of the trap, as during time-of-flight the atoms travel far beyond the initial extent of the cloud $(r_x, r_y, r_z) \approx (45{,}48{,}15)$ μm, while the cloud width after TOF is ≈ 82 μmin each direction. We thus obtained the atomic distribution $\rho(r, \theta)$

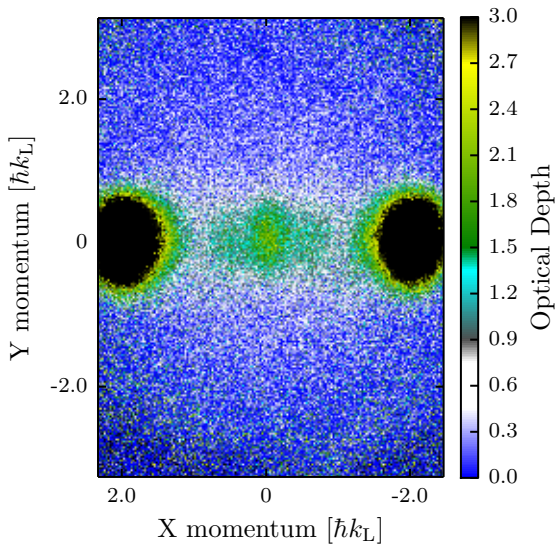

Figures/figure10a.pdf

(a)

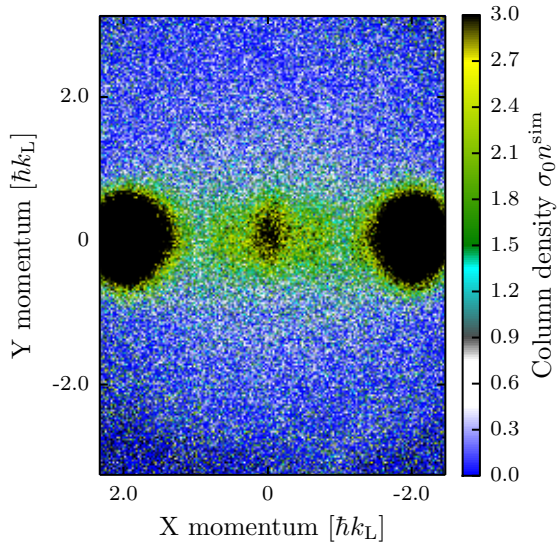

Figures/figure10b.pdf

(b)

Figure 1: An example of our absorption image after 6.8 ms TOF. The 1-D lattice imparts momentum along $\mathbf{e_x}$. The two large clouds on the left and right are the atoms in the $\pm 2k_L$ momentum orders that passed through each other unscattered. The smaller cloud in the center is the atoms that remained in the lowest band of the lattice after pulsing, and thus obtained no momentum. The thin spread of atoms around these clouds is the atoms that underwent scattering. This image was taken coming from below the Feshbach resonance at 20.07 mT. (a) Raw optical depth,

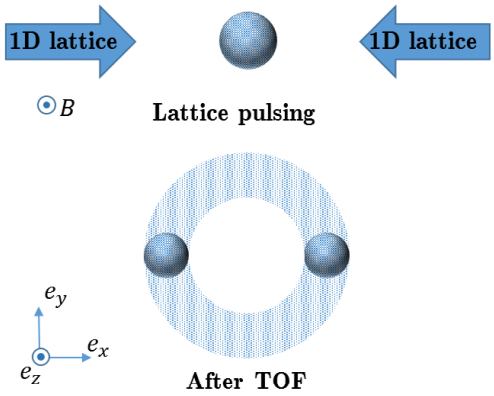

Figures/Picture12.pdf

(a)

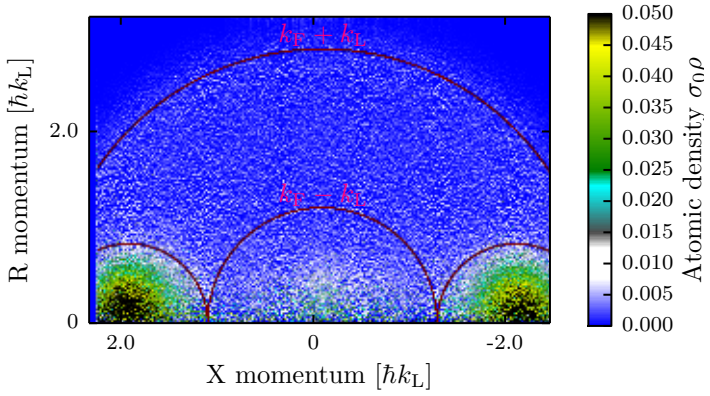

Figures/figure12b.pdf

(b)

Figure 2: (a) Our experimental setup. After time of flight, the two clouds traveling along $\pm\hat{e}_x$ directions have separated and the atoms that underwent a single scattering event were evenly distributed in a scattering halo around the unscattered clouds. The 1-D lattice defined the axis of cylindrical symmetry. (b) Inverse Abel transformed image. The atoms within the Fermi momentum k_F of each unscattered cloud center are in the unscattered region and counted towards the total unscattered number. The atoms outside the radius $k_\mathrm{L} - k_\mathrm{F}$ but inside $k_\mathrm{L} + k_\mathrm{F}$ but outside the unscattered region are counted towards the number of single scattered atoms.

as a function of r, the radial distance from the scattering center, and θ, the angle between r and symmetry axis $\mathbf{e_x}$, integrated over ϕ, the azimuthal angle around the x axis.

We then extracted the number of scattered atoms N_{scat} as a fraction of the total atom number N_{tot} for each image, as shown in Fig. 2(b). The unscattered atom number was the number of atoms in the two unscattered clouds. The number of atoms that underwent a single scattering event was the number of atoms outside the Fermi radius of the unscattered clouds, but inside the arc created by rotating the Fermi momentum k_{F} around the original center of the cloud (red arcs in Fig. 2(b)). For both the scattered and unscattered numbers, we accounted for atoms that fell outside the field of view of our camera by multiplying the counted atom number by a factor of the total area as defined by the radii divided by the visible area on the camera. The atoms in the center region were not counted as they were originally in the zero momentum state and could not contribute to the scattering halo under study.

We fit the fraction of scattered atoms versus the total atom number for each of the 15 images taken at the same bias magnetic field to a line constrained to be zero at zero. The slope of this fit was taken to be the value of $N_{\text{scat}}/N_{\text{tot}}^2$ at that bias magnetic field, and the variance of the fit gave the uncertainty on that data point. This uncertainty reflected our shot to shot number fluctuations, which produced variable atomic densities and thus influence the scattered fraction.

We then deduced the resonant field value B_0 and width of the resonance Δ, the parameters in Eq. (3.1). Since we were in the low energy regime (the atomic

momentum was much smaller than the momentum set by the van der Waals length $k_{\mathrm{L}} + k_{\mathrm{F}} \ll 1/l_{\mathrm{vdW}}$, and we were well below the p-wave threshold temperature [**?**]), the scattering cross-section was given by $\sigma = 4\pi a^2$.

The scattering cross-section σ gives the probability $P_{\mathrm{scat}} = \sigma N/A$ that a single particle will scatter when incident on a cloud of atoms with a surface density of N/A, where A is the cross-sectional area of the cloud and N is the number of atoms in the cloud. In our case, each half of the initial cloud, with atoms number $N_{\mathrm{tot}}/2$, is incident on the other half. Thus, the number of expected scattering events is $N_{\mathrm{scat}} = (N_{\mathrm{tot}}/2)\sigma(N_{\mathrm{tot}}/2) = \sigma N_{\mathrm{tot}}^2/4A$. Assuming A is constant for all our data, we can define a fit parameter $b_0 = 4\pi a_{\mathrm{bg}}^2/4A$, where a_{bg} is the background scattering length. We can thus adapt Eq. (3.1) to obtain the fit function

$$\frac{N_{\mathrm{scat}}}{N_{\mathrm{tot}}^2} = b_0 \left(1 - \frac{\Delta}{B - B_0}\right)^2 + C. \tag{3.2}$$

We found that our imaging noise skewed towards the positive, giving rise to a small background offset. We accounted for this in our fit by including a constant offset parameter C.

3.4 Results

Our final data is presented in Fig. 3. The red curve depicts a best fit of the model given in Eq. (3.2). The fit parameters we extracted were $\Delta = 1(5)$ mT, $B_0 = 20.206(15)$ mT, $b_0 = 5(3) \times 10^{-3}$ and $C = 8(1) \times 10^{-4}$. To obtain the fit, we used data taken by approaching the resonance from above for points above where we expected the resonance to be and data taken approaching the resonance from

below for points below. We also excluded from the fit data points very near the resonance, as there the assumption $\sigma\rho \ll 1$, where ρ is the atom number per unit area, is no longer valid and the problem must be treated hydrodynamically.

The accepted values for the ^{40}K s-wave Feshbach resonance for the $|9/2, -9/2\rangle$ and $|9/2, -7/2\rangle$ states are $B_0 = 20.210(7)$ mT and $\Delta = 0.78(6)$ mT [**?**], which is in good agreement with our findings. Some potential sources of systematic uncertainty that we did not account for include scattering with atoms that did not receive a momentum kick from the lattice pulsing or the impact of multiple scattering events.

3.5 Conclusion

We studied the effects of recoil-induced detuning effects on absorption images and found an optimal imaging time of ≈ 40 μs for ^{40}K atoms for noise minimization after corrections. We use these results to observe s-wave scattering halos of the Fermi gas around the ≈ 20.2 mT Feshbach resonance and directly verified the resonance location and width. Our analysis can be used in any absorption imaging application where SNR optimization is critical.

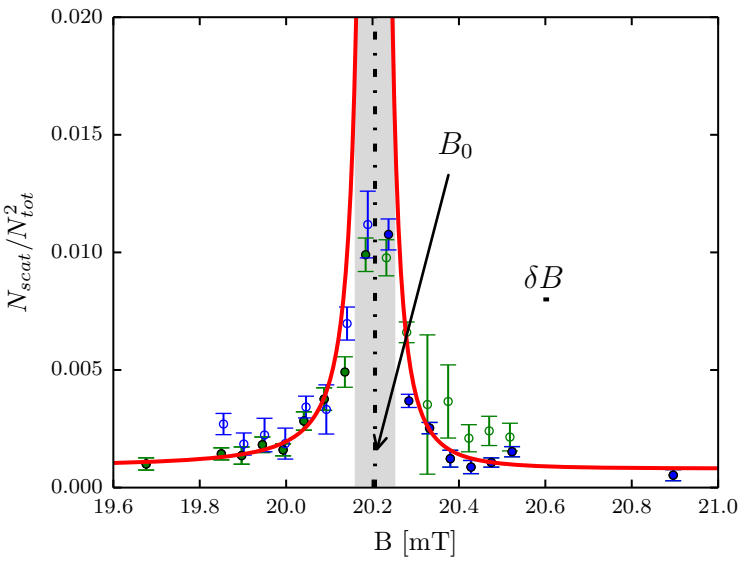

Figures/figure11.pdf

Figure 3: Normalized scattered population plotted versus bias field B. Green dots represent data taken coming from below the resonance, and blue dots represent the data taken coming from above the resonance. The red curve depicts the best fit, where data coming from above the resonance was used above the resonance and data coming from below the resonance was used below the resonance to create the fit; the unused data points are indicated by hollow dots. The regime where the scattering length is likely large enough for the atoms to behave hydrodynamically is shaded in gray, and data points in that area were also excluded from the fit. Resonant field value B_0 as found in this work and our systematic uncertainty in the bias magnetic field δB_0 are indicated.

Bibliography

[1] G.P. Agrawal, *Nonlinear Fiber Optics* (Academic Press, San Diego, CA, 2001), Chap. 1.

[2] N. Bloembergen, *Nonlinear Optics* (Benjamin, Reading, MA, 1977).

[3] Y.R. Shen, *Principles of Nonlinear Optics* (Wiley, New York, 1984).

[4] P.N. Butcher and D.N. Cotter, *The Elements of Nonlinear Optics* (Cambridge University Press, Cambridge, UK, 1990).

[5] R.W. Boyd, *Nonlinear Optics* (Academic Press, San Diego, CA, 1992).

[6] A.C. Newell and J.V. Moloney *Nonlinear Optics (Advanced Topics in the Interdisciplinary Mathematical Sciences)* (Westview Press, Boulder, CO, April 1992).

[7] D. Marcuse,*Light Transmission Optics* (Van Nostrand Reinhold, New York, 1982), Chaps. 8 and 12.

[8] G.P. Agrawal, *Nonlinear Fiber Optics* (Academic Press, San Diego, CA, 2001), Chap. 2.

[9] P. Diament, *Wave Transmission and Fiber Optics* (Macmillan, New York, 1990).

[10] V.E. Zakharov and A.Shabat, Sov. Phys. JETP **34**, 62 (1972)

[11] R.H. Hardin and F.D. Tappert, SIAM Rev. Chronicle **15**, 423 (1973).

[12] R.A.Fisher and W.K. Bischel, Appl. Phys. Lett. **23**, 661 (1973); J. Appl. Phys **46**, 4921 (1975).

[13] J.W. Cooley and J.W. Tukey, Math. Comput. **19**, 297 (1965).

[14] R. Trebino, D.J. Kane, "Using phase retrieval to measure the intensity and phase of ultrashort pulses: frequency resolved optical gating," J. Opt. Soc. Am. B **10**, 1101 (1993).

[15] D.J. Kane, R. Trebino, "Characterization of Arbitrary Femtosecond Pulses Using Frequency-Resolved Optical Gating," IEEE J. Quant. Elect. **29**, 571 (1993).

[16] D.J. Kane, R. Trebino, "Single-shot measurement of the intensity and phase of an arbitrary ultrashort pulse by using frequency-resolved optical gating," Opt. Lett. **10**, 1101 (1993).

[17] P. O'Shea, M. Kimmel, X. Gu, R. Trebino, "Highly simplified device for ultrashort-pulse measurement," Opt. Lett. **26**, 932 (2001).

[18] G.P. Agrawal, *Nonlinear Fiber Optics* (Academic Press, San Diego, CA, 2001), Chap. 3.

[19] G.P. Agrawal, *Nonlinear Fiber Optics* (Academic Press, San Diego, CA, 2001), Chap. 4.

[20] G.P. Agrawal, *Nonlinear Fiber Optics* (Academic Press, San Diego, CA, 2001), Chap. 10.

[21] G.P. Agrawal, *Nonlinear Fiber Optics* (Academic Press, San Diego, CA, 2001), Chap. 7.

[22] G.P. Agrawal, *Nonlinear Fiber Optics* (Academic Press, San Diego, CA, 2001), Chap. 6.

[23] R.H. Stolen, E.P. Ippen, and A.R. Tynes, Appl. Phys. Lett. **20**, 62 (1972).

[24] E.P. Ippen and R.H. Stolen, Appl. Phys. Lett. **21**, 539 (1972).

[25] R.G. Smith, Appl. Opt. **11**, 2489 (1972).

[26] G.P. Agrawal, *Nonlinear Fiber Optics* (Academic Press, San Diego, CA, 2001), Chap. 9.

[27] G.P. Agrawal, *Nonlinear Fiber Optics* (Academic Press, San Diego, CA, 2001), Chap. 8.

[28] D.L. Hart, Arthur F. Judy, Rajarshi Roy and James W. Beletic, Phys. Rev. E **57**, 4757 (1998); D.L. Hart, Arthur F. Judy, T.A.B. Kennedy, Rajarshi Roy and K. Stoev, Phys. Rev. A **50**, 1807 (1994).

[29] K. Ito, *Lectures on Stochastic Processes* (Tata Institute of Fundamental Research, Bombay, 1960).

[30] R.L. Stratanovich, *Topics in the Theory of Random Noise*, Vols I. and II. (Gordon & Breach, New York, 1963).

[31] H. Risken, *The Fokker-Planck Equation* (Springer-Verlag, Berlin, 1989).

[32] M.J. Werner and P.D. Drummond, J. Comput. Phys. **132**, 312 (1997).

[33] P.D. Drummond and I.K. Mortimer, J. Comput. Phys. **93**, 144 (1991).

[34] S.J. Carter, Phys. Rev. A. **51**, 3274 (1995).

[35] J.R. Thompson and Rajarshi Roy, Phys. Rev. A **43**, 4987 (1991).

[36] W.H. Press, S.A. Teukolsky, W.T. Vetterling and B.P. Flannery, *Numerical Recipes in Fortran: The Art of Scientific Computing* (Cambridge University Press, Cambridge, 1992).

[37] C. Headley, G.P. Agrawal, IEEE J. Quantum Electron. **QE-31**, 2058 (1995), C. Headley, G.P. Agrawal J. Opt. Soc. Am. B. **13**, 2170 (1995).

[38] S.H. Perlmutter, M.D. Levenson, R.M. Shelby and M.B. Weisman, Phys. Rev. Lett. **61** 1388, 1988.

[39] F. Kh. Abdullaev, J.H. Hensen, S. Bischoff and M.P. Sorensen, J. Opt. Soc. Am. B. **15**, 2424 (1998); F. Kh. Abdullaev, J.G. Caputo, and Nikos Flytzanis, Phys. Rev E. **50**, 1552 (1994).

[40] William H. Glenn, IEEE J. Quantum Electron. **QE-25**, 1218 (1989).

[41] R. Trebino. *Frequency-Resolved Optical Gating: The Measurement of Ultrashort Laser Pulses* (Kluwer Academic 2002).

[42] G.P. Agrawal *Nonlinear Fiber Optics* (Academic, San Diego, 2001).

[43] J.M. Dudley, X. Gu, L. Xu, M. Kimmel, E. Zeek, P. O'Shea, R. Trebino, S. Coen, R.S. Windeler, "Cross-correlation frequency resolved optical gating analysis of broadband continuum generation in photonic crystal fiber: simulations and experiments," Opt. Express **10**, 1215 (2002).

[44] Q.D. Liu, J.T. Chen, Q.Z. Wang, P.P. Ho, and R.R. Alfano, "Single pulse degenerate-cross-phase modulation in a single-mode optical fiber," Opt. Lett. **20**, 542 (1995).

[45] T. Sylvestre, H. Maillotte, E. Lantz, and D. Gindre "Combined spectral effects of pulse walk-off and degenerate cross-phase modulation in birefringent fibers", Journal of Nonlinear Optical Physics and Materials 6, 313-320 (1997).

[46] Q.D. Liu, L. Shi, P.P. Ho, R.R. Alfano, R.J. Essiambre, and G.P. Agrawal, "Degenerate cross-phase modulation of femtosecond laser pulses in a birefringent single-mode fiber," IEEE Photon. Tech. Lett. **9**, 1107 (1997).

[47] F.G. Omenetto, B.P. Luce, D. Yarotski and A.J. Taylor, "Observation of chirped soliton dynamics at l= 1.55 mm in a single-mode optical fiber with frequency-resolved optical gating," Opt. Lett. **24**, 1392 (1999).

[48] F.G. Omenetto, Y. Chung, D. Yarotski, T. Shaefer, I. Gabitov and A.J. Taylor, "Phase analysis of nonlinear femtosecond pulse propagation and self-frequency shift in optical fibers," Opt. Commun. **208**, 191 (2002).

[49] F.G. Omenetto, J.W. Nicholson, B.P. Luce, D. Yarotski, A.J. Taylor, "Shaping, propagation and characterization of ultrafast pulses in optical fibers," Appl. Phys. B **70**[Suppl.], S143 (2000).

[50] N. Nishizawa and T. Goto, "Experimental analysis of ultrashort pulse propagation in optical fibers around zero-dispersion region using cross-correlation frequency resolved optical gating," Opt. Express **8**, 328 (2001).

[51] N. Nishizawa and T. Goto, "Trapped pulse generation by femtosecond soliton pulse in birefringent optical fibers," Opt. Express **10**, 256 (2002).

[52] N. Nishizawa and T. Goto, "Characteristics of pulse trapping by use of ultrashort soliton pulses in optical fibers across the zero-dispersion wavelength," Opt. Express **10**, 1151 (2002).

[53] N. Nishizawa and T. Goto, "Ultrafast all optical switching by use of pulse trapping across zero-dispersion wavelength," Opt. Express **11**, 359 (2003).

[54] , K. Ogawa, M.D. Pelusi, "Characterization of ultrashort optical pulses in a dispersion-managed fiber link using two-photon absorption frequency-resolved optical gating," Opt. Commun. **198**, 83-87 (2001).

[55] R.A. Altes, "Detection, estimation, and classification with spectrograms," J. Acoust. Soc. Am. **67**(4), 1232 (1980).

[56] A. Christian Silva, "GRENOUILLE - Practical Issues," unpublished.

[57] J. Garduno-Mejia, A.H. Greenaway, and D.T. Reid, "Designer femtosecond pulses using adaptive optics," Opt. Express **11** 2030 (2003).

[58] P. O'Shea, M. Kimmel, X. Gu, R. Trebino, "Increased-bandwidth in ultrashort-pulse measurement using an angle-dithered nonlinear-optical crystal," Opt. Express **7**, 342 (2000).

[59] P. O'Shea, M. Kimmel, R. Trebino, "Increased phase-matching bandwidth in simple ultrashort-laser-pulse measurements," J. Opt. B **4**, 44 (2002).

[60] S. Akturk, M. Kimmel, P. O'Shea, R. Trebino, "Measuring pulse-front tilt in ultrashort pulses using GRENOUILLE", Opt. Express **11**, 491 (2003).

[61] K. J. Blow, D. Wood, "Theoretical Description of Transient Stimulated Raman Scattering in Optical Fibers," IEEE J. Quant. Elect. **25**, 2665 (1989).

[62] R.H. Stolen, J.P. Gordon, W.J. Tomlinson, J. Opt. Soc. Am. B **6**, 1159 (1989).

[63] P.V. Mamyshev and S.V. Chernikov, Sov. Lightwave Commun. **2**, 97 (1992).

[64] C. Headley III, *Ultrafast Stimulated Raman Scattering in Optical Fibers, Ph.D. Thesis, University of Rochester, NY (1995).*